

Determination of the position of a single nuclear spin from free nuclear precessions detected by a solid-state quantum sensor

Kento Sasaki,¹ Kohei M. Itoh,^{1,2,*} and Eisuke Abe^{2,†}

¹*School of Fundamental Science and Technology, Keio University, 3-14-1 Hiyoshi, Kohoku-ku, Yokohama 223-8522, Japan*

²*Spintronics Research Center, Keio University, 3-14-1 Hiyoshi, Kohoku-ku, Yokohama 223-8522, Japan*



(Received 31 May 2018; published 13 September 2018)

We report on a nanoscale quantum sensing protocol which tracks a free precession of a single nuclear spin and is capable of estimating an azimuthal angle—a parameter which standard multipulse protocols cannot determine—of the target nucleus. Our protocol combines pulsed dynamic nuclear polarization, a phase-controlled radio-frequency pulse, and a multipulse ac sensing sequence with a modified readout pulse. Using a single nitrogen-vacancy center as a solid-state quantum sensor, we experimentally demonstrate this protocol on a single ^{13}C nuclear spin in diamond and uniquely determine the lattice site of the target nucleus. Our result paves the way for magnetic resonance imaging at the single-molecular level.

DOI: [10.1103/PhysRevB.98.121405](https://doi.org/10.1103/PhysRevB.98.121405)

Nuclear magnetic resonance (NMR) spectroscopy is an analytical technique extensively used in chemistry, biology, and medicine. It achieves sub-ppm spectral resolutions to provide a wealth of information on the structure and chemical environment of molecules, but requires at least nanoliter-volume analytes containing an ensemble of identical nuclei, due to the insensitive induction detection the technique relies on. In recent years, single isolated electron spins in solids, most prominently those associated with nitrogen-vacancy (NV) centers in diamond [1–3], have emerged as atomic-scale quantum sensors capable of detecting weakly coupled external nuclei in as small as zeptoliter volumes, a dramatic decrease compared with conventional NMR [4–6]. Furthermore, various NMR protocols, in which a train of properly timed microwave pulses interrogates precessing nuclear spins via the interaction with the sensor electron spin, have been devised and applied to external nuclei, demonstrating identifications of isotopes [7–9], detection of single protons [10], spectroscopy of single proteins [11], spectral resolution approaching that of conventional NMR [12,13], and so on [14–17]. A far-reaching yet natural goal of this line of research is a chemical structure analysis at the single-molecular level, i.e., the determination of chemical identities and locations of the constituent nuclei in a single molecule.

For nuclei dipolarly coupled with a sensor, the knowledge of the hyperfine parameters A_{\parallel} and A_{\perp} (the parallel and perpendicular components, respectively) translates to the coordinate parameters r and θ , the distance from the sensor and the tilt (polar angle) from the applied static magnetic field \mathbf{B}_0 , respectively, owing to the form of the interaction $\propto (3 \cos^2 \theta - 1)/r^3$ or $3 \cos \theta \sin \theta/r^3$ [Fig. 1(a), left]. ^{13}C nuclei ($I = \frac{1}{2}$) in diamond sensed by the NV electronic spin ($S = 1$) have served as a canonical testbed for various NMR protocols to

characterize the hyperfine parameters [3,18–25]. For instance, in correlation spectroscopy, a multipulse sequence is repeated with the interval of t_{corr} , during which a target nuclear spin evolves freely. Boss *et al.* demonstrated that, by engineering the Hamiltonian during the free nuclear precession, both A_{\parallel} and A_{\perp} can be estimated with high precision [24]. The information that is still missing in order to *uniquely* determine the position of a target nuclear spin is the azimuthal angle ϕ [26–28], which, due to the symmetry of the interaction, does not formally appear in the Hamiltonian.

In this Rapid Communication, we show that the azimuthal angle can be determined by a multipulse protocol combined with dynamic nuclear polarization (DNP) and radio-frequency (rf) control of a target spin. As a proof of principle, we apply this protocol to the NV- ^{13}C -coupled system, and uniquely assign the lattice site that the ^{13}C nucleus sits in, even when multiple sites equivalent to it exist.

Our protocol proceeds as follows [see Figs. 1(b)–1(g) for the pulse sequences used]. The target nuclear spin is first polarized by transferring the polarization of the sensor electron spin using a multipulse sequence called PulsePol [29], and is tipped to the xy plane by an rf $\pi/2$ pulse. The dipolar field experienced by this tipped nuclear spin is dependent on ϕ ; an example to appreciate this is that, when two nuclear spins are located on opposite sides of the sensor, the directions of the dipolar fields are also opposite [Fig. 1(a), middle]. A subsequent free precession of each nuclear spin carries this information as the initial phase of the oscillation [Fig. 1(a), right].

A central issue that must be addressed in this scenario is how to detect the phase of a nuclear precession. Here, we consider a particular example in which $|m_S = 0\rangle$ and $|m_S = -1\rangle$ sublevels of the NV spin serve respectively as $|0\rangle$ and $|1\rangle$ of the sensor two-level system, but the concept is general. To detect a dynamics of a single nuclear spin, the sensor spin is prepared in a superposition of $|m_S = 0\rangle$ and $|m_S = -1\rangle$, and is subject to a Carr-Purcell (CP) sequence [30] consisting of $N \pi$ pulses equally separated by τ [Fig. 1(b)]. Because only

*kitoh@appi.keio.ac.jp

†e-abe@keio.jp

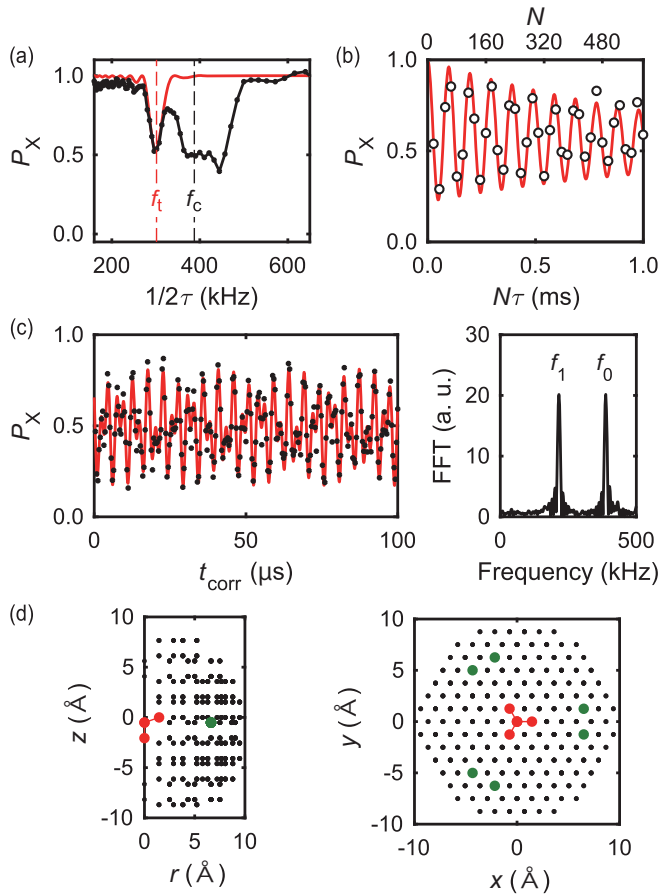


FIG. 2. (a) NMR spectrum taken by the CP sequence ($N = 16$). $f_c = 387.5$ kHz and $f_i = 301.6$ kHz. (b) CP sequence as N is incremented ($\tau = 1.6875$ μ s). (c) Correlation spectroscopy and its Fourier transform. $f_0 = 387.5$ kHz and $f_1 = 215.6$ kHz. In (a)–(c), the red solid lines are simulations using the estimated values of A_{\parallel} and A_{\perp} . (d) Map of the diamond lattice. The x , y , and z axes are parallel to the $[\bar{1}\bar{1}2]$, $[1\bar{1}0]$, and $[\bar{1}\bar{1}1]$ crystallographic directions, respectively. The black dots represent carbon sites, and the green dots are the candidate sites of the ^{13}C nucleus examined. It is assumed that the vacancy site locates above the nitrogen site, and the origin is taken 0.75 Å above the vacancy site [32].

are observing a single nuclear spin and not multiple nuclear spins with the same hyperfine parameters [32].

We further analyze this ^{13}C nucleus by correlation spectroscopy [Fig. 1(c)]. Figure 2(c) shows a modulated oscillation as increasing t_{corr} , and its Fourier transformation reveals two peaks at $f_0 = 387.5$ kHz and $f_1 = 215.6$ kHz. f_0 corresponds exactly to f_c , and therefore results from the coupling with $|m_S = 0\rangle$. On the other hand, $|m_S = -1\rangle$ exerts the hyperfine field on the nuclear spin, shifting its precession frequency. The target nuclear spin is properly probed because $(f_0 + f_1)/2 = 301.55$ kHz $= f_i$, and the negative shift $(f_1 - f_0 < 0)$ suggests negative A_{\parallel} . Combining these results, we deduce $A_{\parallel} = -173.1$ kHz and $A_{\perp} = 22.3$ kHz with an accuracy of about 0.1 kHz [32].

It should be noted that, unlike the case of external nuclear spins, A_{\parallel} and A_{\perp} estimated here are not purely dipolar in

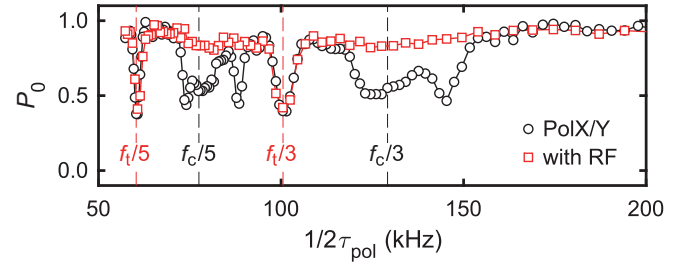


FIG. 3. Demonstration of PulsePol on both nuclear spins (\circ) and on a single, selectively addressed nuclear spin (\square).

nature due to the presence of a relatively strong contact hyperfine interaction. This usually complicates the direct estimation of the coordinate parameters r and θ from A_{\parallel} and A_{\perp} . However, the estimated values are accurate enough to be compared with theoretical calculations. Nizovtsev *et al.* have recently performed an extensive density functional theory (DFT) simulation of a $\text{C}_{510}[\text{NV}]\text{H}_{252}$ cluster [33]. From their list of hyperfine parameters for 510 carbon sites, we find that six sites labeled as C218, C226, C230, C240, C280, and C282 show close agreement with the experimental values. The hyperfine parameters of these sites are, in kHz units, $(A_{\parallel}, A_{\perp}) = (-175.4, 21.7)$, $(-176.7, 21.7)$, $(-174.7, 21.7)$, $(-177.1, 21.9)$, $(-173, 22)$, and $(-173.4, 22.1)$, respectively [average: $(-175.1 \pm 2.1, 21.9 \pm 0.2)$]. The positions of these candidate sites are given in Fig. 2(d). In all cases, we obtain $r = 6.84$ Å and $\theta = 94.8^\circ$ [32].

The next task is to polarize the target nuclear spin. For this, we use a pulsed technique called PulsePol, which is yet another application of Hamiltonian engineering [29]. Figure 1(d) shows two PulsePol sequences labeled as PolY and PolX. One cycle consists of eight pulses with a total duration of $2\tau_{\text{pol}}$. When $2\tau_{\text{pol}} = k/f_n$ is satisfied (k : odd integer; f_n : nuclear Larmor frequency), the average Hamiltonian of a hyperfine-coupled electron-nuclear system becomes proportional to $S_+ I_- + S_- I_+$ (flip-flop) or $S_+ I_+ + S_- I_-$ (flip-flip), driving the polarization transfer between the electron and the nuclei. It is shown that for $k = 3$ PolY (PolX) drives flip-flip (flip-flop), whereas for $k = 5$ PolY (PolX) does flip-flop (flip-flip) [32]. Because the NV spin is optically initialized into $m_S = 0$, PolY (PolX) for $k = 3$ polarizes the nuclei into $m_I = -\frac{1}{2}$ ($\frac{1}{2}$). For $k = 5$, the direction of the nuclear polarization becomes opposite.

We test the performance of PulsePol by successive application of PolX and PolY, as shown in Fig. 1(e). The first PolX serves to depolarize the nuclear polarization during a previous run, and the polarization transfer by PolY is read out as a decrease of the $m_S = 0$ polarization (P_0) [34]. The circle (\circ) points in Fig. 3 are the result of this measurement with $N_{\text{pol}} = 5$. Two “replicas” of the NMR spectrum in Fig. 2(a) are clearly observed at $\frac{1}{3}$ and $\frac{1}{5}$ of the NMR conditions, as expected. Furthermore, a single nuclear spin can be selectively polarized by applying the sequence of Fig. 1(f). This sequence works as follows: (1) PolY is executed nine times in order to fully polarize the nuclei. (2) A microwave π pulse drives the NV spin into $|m_S = -1\rangle$. (3) An rf π pulse tuned at $f_i = 215.6$ kHz is applied. The NV spin being $|m_S = -1\rangle$, only the

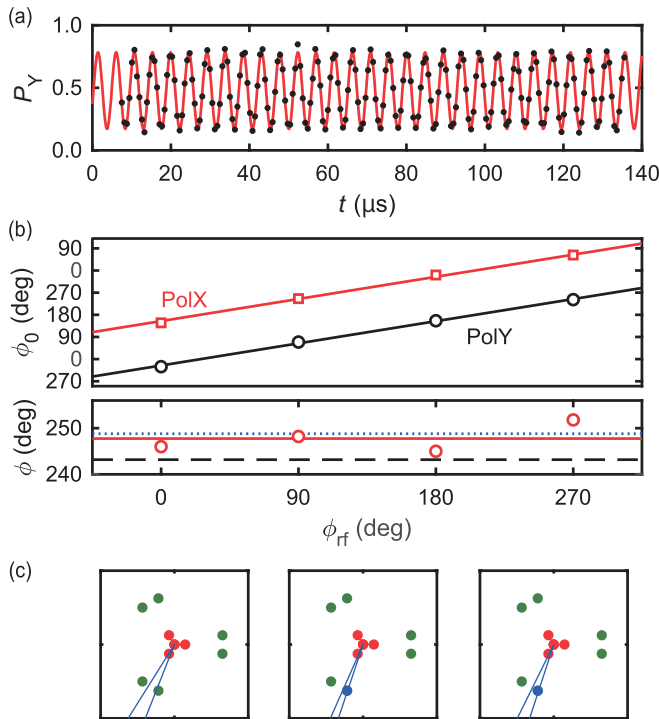


FIG. 4. (a) P_Y as a function of t reveals a free precession of a single nuclear spin. (b) ϕ_0 as a function of ϕ_{rf} (upper panel). The solid lines are linear fits. Estimated ϕ (lower panel). (c) The blue lines indicate the accuracy ranges of ϕ , based on three estimations of $\phi_n(0)$. At most one lattice site (in blue) with $\phi = 250.9^\circ$ falls on the estimated ranges.

target nuclear spin is resonantly flipped by this rf pulse. (4) By the final PolY, the polarization transfer acts only on the flipped nuclear spin, as other nuclei have already been polarized. The square (\square) points in Fig. 3 clearly demonstrate the power of selective polarization; dips are observed only at $f_i/3$ and $f_i/5$, with all other dips almost completely disappeared.

We now demonstrate the protocol of Fig. 1(g) to determine ϕ . Either PolY or PolX is applied with $N_{\text{pol}} = 5$, $N_{\text{rep}} = 5$, and $\tau_{\text{pol}} = 4.9760 \mu\text{s}$. τ_{pol} satisfies $3/(2\tau_{\text{pol}}) = f_i$, for which PolY (PolX) polarizes the target nuclear spin into $m_I = -\frac{1}{2}$ ($\frac{1}{2}$). A phase-controlled selective rf $\pi/2$ pulse tuned at f_1 is applied, followed by the CP sequence with the $(\pi/2)_Y$ readout ($N = 16$, $\tau = 1.6608 \mu\text{s}$). The rf pulse length is chosen to be $102.041 \mu\text{s}$, matched with 22 oscillation periods ($22/f_1$), in order to suppress unwanted phase acquisitions by the rf field along the z axis [32]. Figure 4(a) shows an exemplary trace as changing t . Here, PolY is used, and the waveform of the rf signal is a sine wave, for which we define the rf phase $\phi_{rf} = 270^\circ$. The data are fitted by $A \cos(2\pi f_p t + \phi_0) + B$ (red curve). f_p agrees well with f_1 , confirming that the free precession of the target nuclear spin is indeed detected.

We note that the minimum t is set as $t_0 = 6.872 \mu\text{s}$ in order to avoid an overlap with an rf pulse, whereas our aim here is to estimate the oscillation phase at $t = 0$. To accurately estimate ϕ_0 under this constraint, oscillations should be taken as long as possible. This requires a dauntingly long

measurement time, and at the same time exceedingly high stability of the experimental setup. We therefore choose to undersample the data points for further measurements; by taking less points, t is instead increased up to 1 ms ($< T_1 \approx 5$ ms), and yet the original ϕ_0 is recovered by appropriately setting the measurement parameters [32]. Figure 4(b) shows ϕ_0 determined in this way. The linear dependence on ϕ_{rf} is observed, as expected [32]. ϕ_0 is 180° shifted between PolY and PolX, confirming that the two sequences polarize the nuclear spin into opposite directions. From the fit, we obtain $\phi_0 = \phi_{rf} + 334.0^\circ \pmod{360^\circ}$. On the other hand, if we take into account the azimuthal angle of the rf field in this coordinate and the effect of detuning ($f_p - f_1$), we can estimate $\phi_n(0)$ as $-\phi_{rf} + 89.2^\circ$ [32]. Together, we obtain ϕ as $243.2 \pm 5.3^\circ$ [dashed line in Fig. 4(b)]. $\phi_n(0)$ can be estimated more accurately by simulating the dynamics of the nuclear spin [32]. The simulations give $\phi = 248.8 \pm 2.7^\circ$ (dotted line) or $247.8 \pm 4.1^\circ$ (solid line), marginally dependent on the parameters used. Figure 4(c) shows the accuracy ranges of ϕ determined by these estimations, and there is at most one lattice site that falls on this range; we have been able to pinpoint the lattice site of the target nuclear spin [32].

To summarize, we have described a protocol which tracks a free precession of a single nuclear spin. Combined with DNP and a phase-controlled rf pulse, our method is capable of determining the azimuthal angle of the target nuclear spin. A particular experimental demonstration was performed on a single ^{13}C nuclear spin and its lattice position was uniquely pinpointed. Previously, the position of a single ^{13}C nuclear spin in diamond had been estimated by analyzing NMR spectra taken at three differently oriented \mathbf{B}_0 [22]. When the NV center or other solid-state defects with $S > \frac{1}{2}$ electron spin is used as a sensor, an application of \mathbf{B}_0 misaligned from the sensor quantization axis complicates the analysis. The present protocol circumvents this issue. Looking ahead, we imagine that the present protocol could be employed for three-dimensional mapping of nuclear spins in a single molecule positioned on a near-surface NV sensor [35]. The nuclear-nuclear interactions within the immobilized molecule can be suppressed using dipolar decoupling sequences such as WAHUA and MREV [12,36], which are compatible with our protocol. The protocol can also be combined with the high-resolution spectroscopy method [13,37,38], so that chemical shifts and J couplings could be resolved. Thus, our result paves the way for magnetic resonance imaging at the single-molecular level.

Note added. Recently, we became aware of an article by Zopes *et al.*, which reported a similar method to locate single nuclear spins [39].

The authors thank C. L. Degen, J. Zopes, and J. Boss for helpful discussions, especially on the preparation and calibration of an rf coil, and also for letting us know about their related work [40]. K.S. is supported by JSPS Grant-in-Aid for Research Fellowship for Young Scientists (DC1) No. JP17J05890. K.M.I. is supported by JSPS Grant-in-Aid for Scientific Research (KAKENHI) (S) No. 26220602, JST Development of Systems and Technologies for Advanced Measurement and Analysis (SENTAN), JSPS Core-to-Core Program, and Spintronics Research Network of Japan (Spin-RNJ).

- [1] R. Schirhagl, K. Chang, M. Loretz, and C. L. Degen, Nitrogen-vacancy centers in diamond: Nanoscale sensors for physics and biology, *Annu. Rev. Phys. Chem.* **65**, 83 (2014).
- [2] L. Rondin, J.-P. Tetienne, T. Hingant, J.-F. Roch, P. Maletinsky, and V. Jacques, Magnetometry with nitrogen-vacancy defects in diamond, *Rep. Prog. Phys.* **77**, 056503 (2014).
- [3] E. Abe and K. Sasaki, Tutorial: Magnetic resonance with nitrogen-vacancy centers in diamond—microwave engineering, materials science, and magnetometry, *J. Appl. Phys.* **123**, 161101 (2018).
- [4] H. J. Mamin, M. Kim, M. H. Sherwood, C. T. Rettner, K. Ohno, D. D. Awschalom, and D. Rugar, Nanoscale nuclear magnetic resonance with a nitrogen-vacancy spin sensor, *Science* **339**, 557 (2013).
- [5] T. Staudacher, F. Shi, S. Pezzagna, J. Meijer, J. Du, C. A. Meriles, F. Reinhard, and J. Wrachtrup, Nuclear magnetic resonance spectroscopy on a (5-nanometer)³ sample volume, *Science* **339**, 561 (2013).
- [6] M. Loretz, S. Pezzagna, J. Meijer, and C. L. Degen, Nanoscale nuclear magnetic resonance with a 1.9-nm-deep nitrogen-vacancy sensor, *Appl. Phys. Lett.* **104**, 033102 (2014).
- [7] C. Müller, X. Kong, J.-M. Cai, K. Melentijević, A. Stacey, M. Markham, D. Twitchen, J. Isoya, S. Pezzagna, J. Meijer, J. F. Du, M. B. Plenio, B. Naydenov, L. P. McGuinness, and F. Jelezko, Nuclear magnetic resonance spectroscopy with single spin sensitivity, *Nat. Commun.* **5**, 4703 (2014).
- [8] T. Häberle, D. Schmid-Lorch, F. Reinhard, and J. Wrachtrup, Nanoscale nuclear magnetic imaging with chemical contrast, *Nat. Nanotechnol.* **10**, 125 (2015).
- [9] S. J. DeVience, L. M. Pham, I. Lovchinsky, A. O. Sushkov, N. Bar-Gill, C. Belthangady, F. Casola, M. Corbett, H. Zhang, M. Lukin, H. Park, A. Yacoby, and R. L. Walsworth, Nanoscale NMR spectroscopy and imaging of multiple nuclear species, *Nat. Nanotechnol.* **10**, 129 (2015).
- [10] A. O. Sushkov, I. Lovchinsky, N. Chisholm, R. L. Walsworth, H. Park, and M. D. Lukin, Magnetic Resonance Detection of Individual Proton Spins Using Quantum Reporters, *Phys. Rev. Lett.* **113**, 197601 (2014).
- [11] I. Lovchinsky, A. O. Sushkov, E. Urbach, N. P. de Leon, S. Choi, K. De Greve, R. Evans, R. Gertner, E. Bersin, C. Müller, L. McGuinness, F. Jelezko, R. L. Walsworth, H. Park, and M. D. Lukin, Nuclear magnetic resonance detection and spectroscopy of single proteins using quantum logic, *Science* **351**, 836 (2016).
- [12] N. Aslam, M. Pfender, P. Neumann, R. Reuter, A. Zappe, F. F. de Oliveira, A. Denisenko, H. Sumiya, S. Onoda, J. Isoya, and J. Wrachtrup, Nanoscale nuclear magnetic resonance with chemical resolution, *Science* **357**, 67 (2017).
- [13] D. R. Glenn, D. B. Bucher, J. Lee, M. D. Lukin, H. Park, and R. L. Walsworth, High-resolution magnetic resonance spectroscopy using a solid-state spin sensor, *Nature (London)* **555**, 351 (2018).
- [14] T. Staudacher, N. Raatz, S. Pezzagna, J. Meijer, F. Reinhard, C. A. Meriles, and J. Wrachtrup, Probing molecular dynamics at the nanoscale via an individual paramagnetic centre, *Nat. Commun.* **6**, 8527 (2015).
- [15] X. Kong, A. Stark, J. Du, L. P. McGuinness, and F. Jelezko, Towards Chemical Structure Resolution with Nanoscale Nuclear Magnetic Resonance Spectroscopy, *Phys. Rev. Appl.* **4**, 024004 (2015).
- [16] V. S. Perunicic, C. D. Hill, L. T. Hall, and L. C. L. Hollenberg, A quantum spin-probe molecular microscope, *Nat. Commun.* **7**, 12667 (2016).
- [17] P. Kehayias, A. Jarmola, N. Mosavian, I. Fescenko, F. M. Benito, A. Laraoui, J. Smits, L. Bougas, D. Budker, A. Neumann, S. R. J. Brueck, and V. M. Acosta, Solution nuclear magnetic resonance spectroscopy on a nanostructured diamond chip, *Nat. Commun.* **8**, 188 (2017).
- [18] N. Zhao, J.-L. Hu, S.-W. Ho, J. T. K. Wan, and R. B. Liu, Atomic-scale magnetometry of distant nuclear spin cluster via nitrogen-vacancy spin in diamond, *Nat. Nanotechnol.* **6**, 242 (2011).
- [19] A. Laraoui, J. S. Hodges, C. A. Ryan, and C. A. Meriles, Diamond nitrogen-vacancy center as a probe of random fluctuations in a nuclear spin ensemble, *Phys. Rev. B* **84**, 104301 (2011).
- [20] S. Kolkowitz, Q. P. Unterreithmeier, S. D. Bennett, and M. D. Lukin, Sensing Distant Nuclear Spins with a Single Electron Spin, *Phys. Rev. Lett.* **109**, 137601 (2012).
- [21] T. H. Taminiau, J. J. T. Wagenaar, T. van der Sar, F. Jelezko, V. V. Dobrovitski, and R. Hanson, Detection and Control of Individual Nuclear Spin Using a Weakly Coupled Electron Spin, *Phys. Rev. Lett.* **109**, 137602 (2012).
- [22] N. Zhao, J. Honert, B. Schmid, M. Klas, J. Isoya, M. Markham, D. Twitchen, F. Jelezko, R. B. Liu, H. Fedder, and J. Wrachtrup, Sensing single remote nuclear spins, *Nat. Nanotechnol.* **7**, 657 (2012).
- [23] A. Laraoui, F. Dolde, C. Burk, F. Reinhard, J. Wrachtrup, and C. A. Meriles, High-resolution correlation spectroscopy of ¹³C spins near a nitrogen vacancy centre in diamond, *Nat. Commun.* **4**, 1651 (2013).
- [24] J. M. Boss, K. Chang, J. Armijo, K. Cujia, T. Rosskopf, J. R. Maze, and C. L. Degen, One- and Two-Dimensional Nuclear Magnetic Resonance Spectroscopy with a Diamond Quantum Sensor, *Phys. Rev. Lett.* **116**, 197601 (2016).
- [25] T. Rosskopf, J. Zopes, J. M. Boss, and C. L. Degen, A quantum spectrum analyzer enhanced by a nuclear spin memory, *npj Quantum Inf.* **3**, 33 (2017).
- [26] A. Laraoui, D. Pagliero, and C. A. Meriles, Imaging nuclear spins weakly coupled to a probe paramagnetic center, *Phys. Rev. B* **91**, 205410 (2015).
- [27] Z.-Y. Wang, J. F. Haase, J. Casanova, and M. B. Plenio, Positioning nuclear spins in interacting clusters for quantum technologies and bioimaging, *Phys. Rev. B* **93**, 174104 (2016).
- [28] Z.-Y. Wang, J. Casanova, and M. B. Plenio, Delayed entanglement echo for individual control of a large number of nuclear spins, *Nat. Commun.* **8**, 14660 (2017).
- [29] I. Schwartz, J. Scheuer, B. Tratzmiller, S. Müller, Q. Chen, I. Dhand, Z.-Y. Wang, C. Müller, B. Naydenov, F. Jelezko, and M. B. Plenio, Robust optical polarization of nuclear spin baths using Hamiltonian engineering of NV centre quantum dynamics, *Sci. Adv.* **4**, eaat8978 (2018).
- [30] H. Y. Carr and E. M. Purcell, Effect of diffusion on free precession in nuclear magnetic resonance experiments, *Phys. Rev.* **94**, 630 (1954).
- [31] T. H. Taminiau, J. Cramer, T. van der Sar, V. V. Dobrovitski, and R. Hanson, Universal control and error correction in multi-qubit spin registers in diamond, *Nat. Nanotechnol.* **9**, 171 (2014).
- [32] See Supplemental Material at <http://link.aps.org/supplemental/10.1103/PhysRevB.98.121405> for detailed information.

- [33] A. P. Nizovtsev, S. Y. Kilin, A. L. Pushkarchuk, V. A. Pushkarchuk, S. A. Kuten, O. A. Zhikol, S. Schmitt, T. Uden, and F. Jelezko, Non-flipping ^{13}C spins near an NV center in diamond: Hyperfine and spatial characteristics by density functional theory simulation of the $\text{C}_{510}[\text{NV}]\text{H}_{252}$ cluster, *New J. Phys.* **20**, 023022 (2018).
- [34] J. Scheuer, I. Schwartz, S. Müller, Q. Chen, I. Dhand, M. B. Plenio, B. Naydenov, and F. Jelezko, Robust techniques for polarization and detection of nuclear spin ensembles, *Phys. Rev. B* **96**, 174436 (2017).
- [35] J. Wrachtrup, F. Jelezko, B. Grotz, and L. McGuinness, Nitrogen-vacancy centers close to surfaces, *MRS Bull.* **38**, 149 (2013).
- [36] U. Haeberlen, *High Resolution NMR in Solids Selective Averaging* (Academic, New York, 1976).
- [37] S. Schmitt, T. Gefen, F. M. Stürner, T. Uden, G. Wolff, C. Müller, J. Scheuer, B. Naydenov, M. Markham, S. Pezzagna, J. Meijer, I. Schwarz, M. Plenio, A. Retzker, L. P. McGuinness, and F. Jelezko, Submillihertz magnetic spectroscopy performed with a nanoscale quantum sensor, *Science* **356**, 832 (2017).
- [38] J. M. Boss, K. S. Cujia, J. Zopes, and C. L. Degen, Quantum sensing with arbitrary frequency resolution, *Science* **356**, 837 (2017).
- [39] J. Zopes, K. Herb, K. S. Cujia, and C. L. Degen, Three-dimensional nuclear spin positioning using coherent radio-frequency control, [arXiv:1807.04559](https://arxiv.org/abs/1807.04559).
- [40] J. Zopes, K. S. Cujia, K. Sasaki, J. M. Boss, K. M. Itoh, and C. L. Degen, Three-dimensional localization spectroscopy of individual nuclear spins with sub-Angstrom resolution, [arXiv:1806.04883](https://arxiv.org/abs/1806.04883).